ORIGINAL ARTICLE

A clean and sustainable CO_2 storage method in construction materials

B. Balinee · P. G. Ranjith [ID] **· Herbert E. Huppert**

Abstract Production of building materials emits 11% of global carbon dioxide (CO_2) emission. The greenhouse gas emission from the construction industry has been tried to mininmize from early 1980s; but after four decades of development, it is not fully sustainable. Cement is the second most consumed material in the world, after water and cement production contributes for 8% of global CO_2 emission. We produced a *greener cement* from abundantly available waste: fly ash, blast furnace lag, and rice husk ash to significantly minimize the greenhouse gas emission. Discarded aluminium foil becomes one of most landfilling waste that has high potential for recycling. On other hand, cement carbonation is a curing method that stores significant amount of CO_2 into cement with lesser cost and energy compared to commercial carbon sequestration. Therefore, we incorporate aluminium foil waste and CO_2 waste from industry to improve the engineering and environmental performance of the cement. We compared changes in carbonation when using gaseous carbon dioxide (gCO_2) and supercritical carbon dioxide ($scCO_2$) and found that the $scCO_2$ condition achieves higher compressive strength and yielded a stronger barrier against leaching. Hence, this carbon cured cement can be widely used in underground applications, where the heavy metal leaching is a critical issue. Projections show our greener cement reducing CO_2 emission by 55% compared to Portland cement and reducing direct costs by 35%. Also, our cement ultimately reduces hydrogen gas demand by recycling aluminium, which releases pure hydrogen during the production process, and this effect reduces annual CO_2 emission by 35 million tonnes from this hydrogen production alone. Adopted globally, the system would permanently store 72 million tonnes of CO_2 in a stable composite annually. On whole, our cement production significantly reduces the energy requirement for cement manufacturing and releases future energy, hydrogen gas, as by product.

Article highlights

- The Greener cement is produced with 55% less in CO_2 emission and 35% less in cost compared to OPC.
- Our cement production releases 2 million ton of H2 yearly and it could reduce 35 million ton of CO_2 emitting from conventional H2 production.
- Annually, 72 million ton of atmospheric CO_2 can be utilized in cement industry for solving heavy metal leaching.

B. Balinee · P. G. Ranjith (✉)
Deep Earth Energy Laboratory, Department of Civil Engineering, Australian Academy of Technology and Engineering, Monash University, Building 60, Melbourne, VIC 3800, Australia
e-mail: ranjith.pg@monash.edu

H. E. Huppert
Institute of Theoretical Geophysics, King's College, Cambridge CB2 1ST, UK

1 Introduction

The construction industry is responsible for 11% of global CO_2 emissions, including 5% from the cement industry alone ((IEA), 2019b; Amato, 2013). Globally, 1.32 Gt of CO_2 was emitted from cement production in 2014 (Davis et al., 2018); and over the next 30 years cement demand is expected to rise by 12–23% due to population growth ((IEA), 2018). Emissions from infrastructure developments could increase global temperatures by 2 °C (Churkina et al, 2020). In the face of increased demand, conventional additions to cement are being replaced by lower-emission *supplementary cement materials* (SCMs) such as fly ash (FA), blast furnace slag, rice husk ash (RHA), and waste glass (Habert et al., 2020).

"It's not easy being green," wrote Richard A. Clarke (1994), former chairman and chief executive officer of Pacific Gas and Electric (California). SCMs are already put to work as active precursors, but these commercial alkali activators (Cheng-Yong et al., 2017) are environmentally unfriendly and consume excessive energy (Fawer et al., 1999; Mohajerani et al., 2019). For example, sodium silicate as an alkali source accounts for estimated emissions of 1.51 kg carbon dioxide equivalent (CO_2-eq) per kilogram (Turner & Collins, 2013). To improve the rheological and mechanical performance of cementitious materials, industry experts are proposing (and already using) commercial additives such as superplasticizer and retarders, along with fillers such as hollow microspheres and fibres of polyvinyl alcohol (PVA) (Aslani & Wang, 2019; Khalifeh et al., 2014; Şahmaran et al., 2011; Scrivener & Capmas, 1998). Analysis of superplasticizers estimates emissions at around 2 kg CO_2-eq/kg (Latawiec et al, 2018); and production of PVA accounts for 1.73 kg CO_2-eq/kg (Patel et al., 2005).

In our work we used RHA as an alternative to commercial silicate, and discarded aluminium foil (Al) as alternatives to commercial additives. Only 25% of the world's annual 70 million tonnes yield of RHA is currently recycled (Venkatanarayanan & Rangaraju, 2015), leaving > 50 million tonnes to landfill. Discarded aluminium foil is abundant in waste streams

and can be 100% recyclable, but it has little acceptance in the recycling industry since it is dirtier than aluminium cans and could damage processing equipment. So each year 20,000 tonnes of used Al foil is lost to landfill or incinerated (Osman, 2017). Here we show that discarded Al foil are potentially viable as replacements for commercial additives in the construction industry.

Our results also show that if industry incorporates waste CO_2 in cement, this would not only improve mechanical properties but also keep a significant amount of CO_2 out of the atmosphere. We analysed how carbonation affects leaching in cement composites made using municipal and industrial waste materials – with either gaseous carbon dioxide (gCO_2) or supercritical carbon dioxide ($scCO_2$). We showed that storage of atmosphere CO_2 in cement would limit the leaching of heavy metal ions (defined as including ions of Mg, Na, Si, etc.) to the environment.

2 Method and materials

2.1 Materials and Sample Preparation

Class F FA and granulated blast furnace slag (GBFS) were sourced from Australian coal power plants and iron refineries, respectively. For our alternative silica source, we purchased RHA (Aslani & Wang). We used analytical grade (99.9%) sodium hydroxide (NaOH) as the alkali source.

In preparing the samples we kept the following parameters constant: FA:GBFS ratio 40:60; liquid:solid ratio 0.48:1; Na_2O:Al_2O_3 molar ratio 1.2:1; H_2O/Na_2O molar ratio 15%. We obtained RHA as a powder with average grain diameter 200 μm. We introduced discarded Al foil together into an 8 M NaOH solution: at an Al/(FA + GBFS) percentage by weight of 0.5%. Cement made with FA, GBFS, RHA, and NaOH is referred as "control"; and cement composites made of FA, GBFS, RHA, NaOH and 0.5% Al is denoted as "0.5Al".

We cast the control mixture in PVC moulds in two different sizes; (1)diameter 20 mm and height 40 mm cylinder (20D), (2) diameter 38 mm and height 76 mm cylinder (38D) since for saturation, small samples were preferred due to limited volume of saturation chamber. 20D samples were used for carbon curing method, and 38D samples were used

Geomech. Geophys. Geo-energ. Geo-resour. (2022) 8:160

Page 3 of 12 **160**

for ambient curing condition (21 ± 2 °C and $50 \pm 10\%$ relative humidity (RH)). After 24 h we demoulded the samples, control (38D) and 0.5Al (38D) samples were kept at ambient condition (air curing) for 7 days, 28 days and 56 days. 20D samples were placed in saturation chambers for carbonation test. To carbonize the samples, we cured the composites under two conditions, gaseous carbon dioxide (gCO_2) and supercritical carbon dioxide ($scCO_2$), for three different curing periods: 7 days, 28 days, and 56 days.

To determine the heavy-metal leaching of the composites with carbonation time, we placed the samples in chambers half-filled with water. We maintained the gCO_2 condition by pressurizing chambers at 5 MPa (room temperature), and the $scCO_2$ condition by pressurizing at 8 MPa (40 °C). To compare carbonation characteristics, we prepared 20D control samples and kept in water medium (water-cured) at room temperature (21 ± 2 °C). Figure 1 shows the set-up arrangements for $scCO_2$ condition.

2.2 Testing methods

2.2.1 Rheological analysis

The plastic viscosity and yield stress of the cement slurries were determined using the ARES-G2 rheometer with a temperature control system following the requirements of ASTM C1749-17. The rheometer was calibrated using the given standard solutions before testing. Three tests were conducted for each samples and the tests were performed after 10 min of mixing. A shear strain rate ramping protocol was adopted starting from 0.1 s^{-1} up to 30 s^{-1} using parallel-plate geometry (Advanced Peltier System (APS) Heat break collars and a plate 25 mm in diameter).

2.2.2 Mechanical strength test

At the end of curing periods, sets of three samples were tested under a series of uniaxial compressive strength tests (UCS) on a Shimadzu 300kN frame at a loading rate of 0.2 mm/min for each testing conditions.
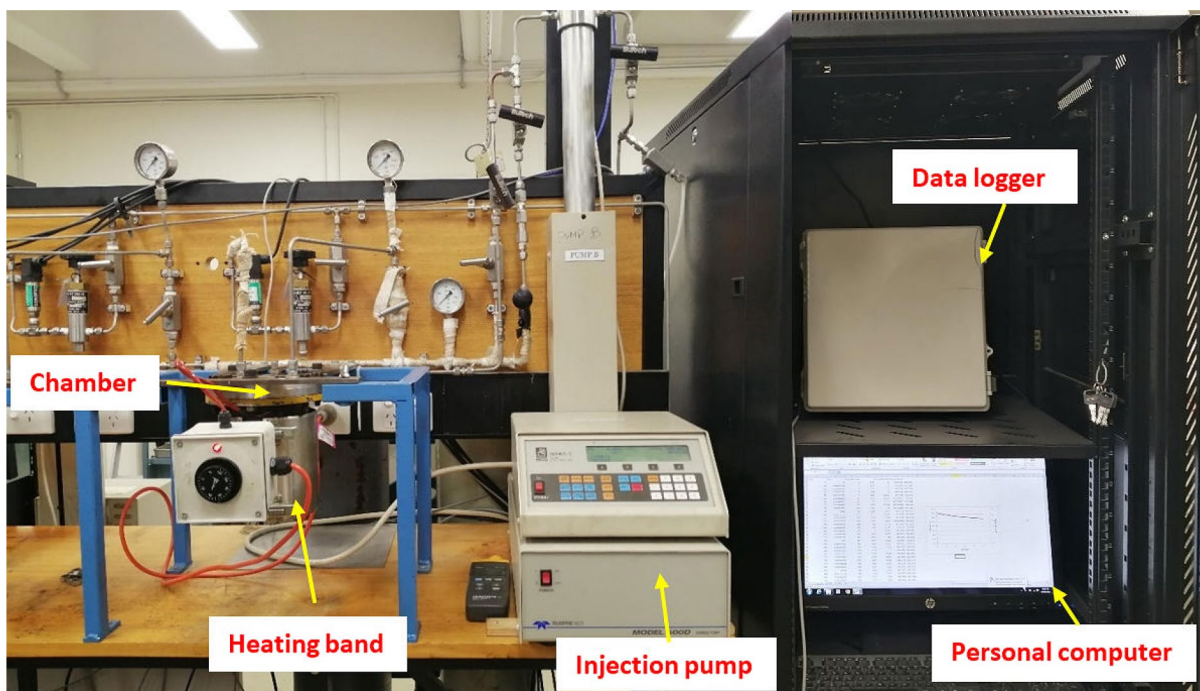
Fig. 1 Experimental set-up for $scCO_2$ condition

2.2.3 Mineral and Microstructural analysis

After the curing period, we traced the changes in mineral phases due to the addition of CO_2 by using X-ray diffraction (XRD) analysis with a Bruker D8 ECO cobalt X-ray diffractometer: Co Kα radiation at 40 kV and 25 mA, range (2θ) 10°–90°, step size 0.02°, and dwell time 0.9 s/step. The divergence slit size was 0.6 mm, and the diffracted signal was detected by a LynEye XE detector.

Scanning electron microscopy (SEM) allowed us to capture microstructural changes. We used FEI Quanta FIB/SEM to obtain microstructural images for identifying hydrates and special features. Samples were scanned under analytical mode at 15.0 kV voltage and 8.0 nA current.

2.2.4 Chemical analysis

At the end of each curing period, we collected the resulting leachate solution from the chambers for tracing the presence of heavy metals through ICP-OES analysis; 24 h before analysis, we added 1% of nitric acid to the samples, arresting any further precipitation.

Table 1 Chemical composition of four raw materials

Component	FA (%)	GBFS (%)	Al foil (%) (Inc, 2017)	RHA (%)
SiO_2	62.7	32.7	–	92.8
Al_2O_3	27.1	13.0	–	0.3
CaO	2.1	43.0	–	0.8
Fe_2O_3	2.6	0.3	–	–
K_2O	1.3	–	–	3.3
MgO	0.4	5.8	–	0.6
SO_3	<0.1	1.4	–	0.2
P_2O_5	0.3	–	–	1.2
TiO_2	1.0	–	–	0.1
MnO	–	0.2	–	–
Na_2O	–	0.4	–	–
S	–	–	–	–
Al	–	–	98.17	–
Other metal (Cu, Si, Fe, Mn, Mg, Zn, Ti)	–	–	1.83	–
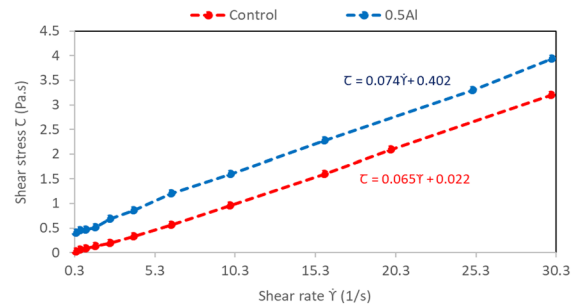
Fig. 3 Variation of viscosity with addition of Al
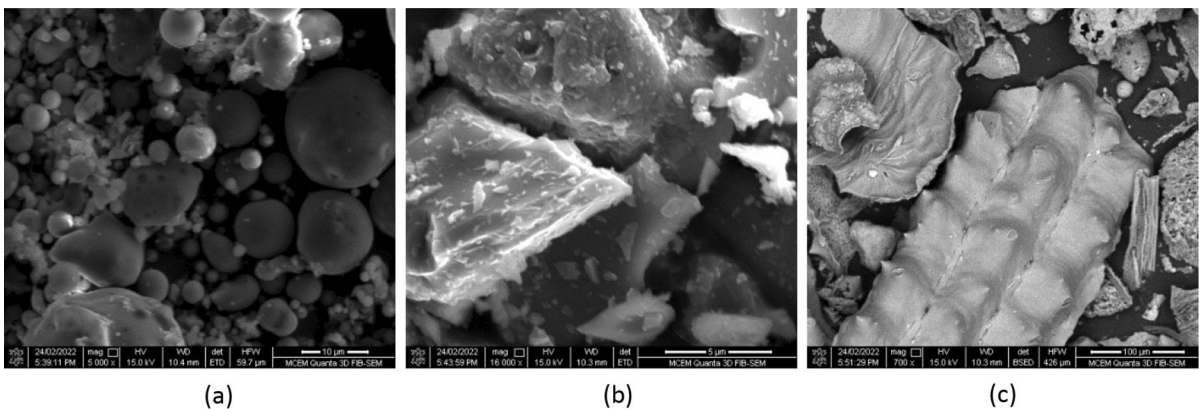
Fig. 2 SEM image of **a** FA; **b** GBFS; **c** RHA
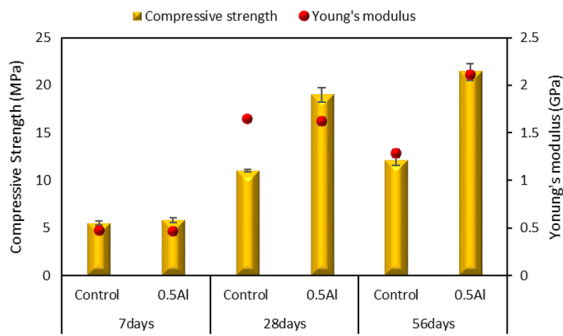
Fig. 4 Variation of Compressive strength and Young's modulus with addition of Al

Fig. 5 Variation of Compressive strength with CO_2 exposure

3 Results and Discussion

3.1 Materials Characterization

Chemical compositions of the FA, GBFS, RHA and Al foil are shown in Table 1. Microstructural image of raw materials are shown on Fig. 2,

3.2 Rheological and mechanical properties

3.2.1 Rheology

Plastic viscosity and yield stress for control and 0.5Al slurries were analysed at 21 °C using rheometer and shown in Fig. 3. Fresh cement slurries were subjected for tested after 10 min of mixing. Viscosity of slurry decrease with shear rate due to non-Newtonian behaviour of slurry (Mohammed, 2018). Bingham-Plastic model ($\tau = \tau_o + \eta\dot{\gamma}$; where τ-shear stress, τ_o -yield-stress, η-plastic viscosity and Υ-shear strain rate) was used to interpret the results (Sun et al. 2017). Plastics viscosity of 0.5Al (0.0742) is higher than that of control (0.065) since addition Al to NaOH accelerates the initial hydration reaction immediately after the cement mixing and further, shear thinning behaviour in 0.5Al enhances.

3.2.2 Mechanical properties of composites

Figure 4 shows the compressive strength and Young's modulus variation of control and 0.5Al with curing period. After 7 days, control and 0.5Al have similar strength value but at end of 28 days curing, 0.5Al

achieves 73% higher strength than control. When the Si/Al is higher than 2.0, increase in Si/Al decreases the mechanical strength of composite (Castillo et al., 2021). As addition of Al reduces the resultant Si/Al ratio to 2.65 from 2.72, 0.5Al composite becomes stronger. Similarly, after 56 days, introduction of Al improves the strength by 77% by accelerating the formation of sodium alumina silicate hydrate gel (NASH).

Young's modulus was calculated according to the variation of stress with strain. Control and 0.5Al have approximately equal stiffness at 7 days and 28 days but at 56 days, stiffness of control sample reduces by 20% that is 80% lower than that of 0.5Al. The significant stiffness reduction of control samples occurs due to the dehydration process where, the incorporation Al in 0.5Al gains higher young modulus and balances the stiffness degradation.

In Fig. 5, compressive strength of water cured and carbonated samples are compared with time. With the curing period, water cured and $scCO_2$ samples gain strength, where no significant changes were observed in gCO_2 samples. Generally, water bath method is highly used in real construction application as it avoids the dehydration process and accelerates the strength development. Therefore, a gradual strength improvement could be noticed in water cured samples with time.

In gCO_2 and $scCO_2$ conditions, sodium ions leach out due to hydrolytic reactions. This effect weaken the alumina silicate skeleton, and affects the stability of the aluminate species (Wan et al., 2020). When the cement is exposed to CO_2, Calcium silica hydrate (CSH) gel starts to degrade to form $CaCO_3$.

160 Page 6 of 12

Geomech. Geophys. Geo-energ. Geo-resour. (2022) 8:160
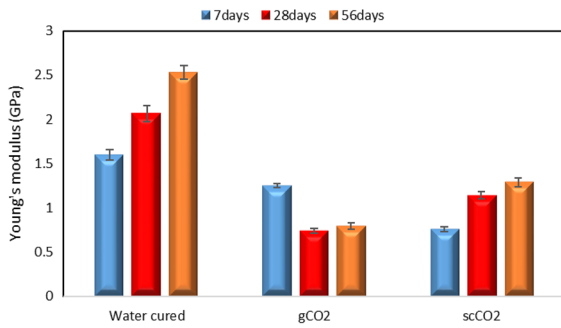
Fig. 6 Variation of Young's modulus with CO_2 exposure

The strength reduction after 7 days causes due to the weaken NASH bond and degradation of CSH. In $ScCO_2$ condition, formed CaCO3 in form of calcite, vaterite and aragonite helps to seal the pores in cement and increases the compressive strength (Kim, 2016). In gCO_2 condition, as rate of formation of $CaCO_3$ is slow, degradation of CSH and continuous sodium leaching start to dominate the changes on mechanical properties and reduce the strength of cement.

Young's modulus was calculated for water cured, gCO_2 and $scCO_2$ and shown in Fig. 6. Young's modulus varies as similar as compressive strength does with time. Stiffness of water cured and $scCO_2$ samples increase with curing period, whereas stiffness of gCO_2 begins to loss with time at 28 days and maintains the same value at 56 days. Due to degradation of CSH and weaken NASH bond, carbonized samples has less stiffness compared to water cured samples.

3.3 Carbon storage in cement

Leachate samples collected at the end of each curing period had different concentrations of alkali ions, evident in the pH values (Table 2). With

Table 2 pH value of leachates

Curing period	pH of leachate		
	gCO_2	$scCO_2$	Atmosphere condition
7 days	10.30	11.00	13.50
28 days	9.03	10.50	13.40
56 days	6.63	7.93	12.60

aging, the leachate pH drops as CO_2 dissolves in water and forms carbonic acid. The rate of reaction also increases with curing (Mi et al., 2021). Significantly, $scCO_2$ conditions result in more alkali-saturated solutions than gCO_2 conditions.

The rate of carbon storage with the period could be evidenced in Fig. 7. Here, carbon stored at 56 days is taken as reference to calculate the weight percentage (wt%: weight of stored CO_2 at selected period/ weight of stored CO_2 at 56 days $\times 100\%$). The CO_2 absorption in the $scCO_2$ at initial stage is higher than gCO_2 as carbonation reaction is accelerated in $scCO_2$ condition but after 20 days, absorption rate in gCO_2 condition is higher than in the $scCO_2$, because formation of nahcolite ($NaHCO_3$) is accelerated with $scCO_2$, maintaining the leachate at a higher pH condition and retarding dissolution of CO_2.

Supercritical condition facilitates 2% (mass of CO_2/mass of composite in %) of carbon storage in the composite, whereas annually 72 million ton of CO_2 can be effectively stored in cement.

Figure 8 shows SEM images of the control, gCO_2, and $scCO_2$ samples after 7, 28, and 56 days of curing. Considerable calcite is evident in both carbonation conditions. With $scCO_2$ the pores are packed with calcite, reducing total porosity. As calcite acts as fillers, the load bearing capacity and stiffness of carbonated samples could further increase. This effect could be validated with the higher compressive strength and stiffness of $scCO_2$ but degradation of CSH and NASH, and heavy leaching of ions make the gCO_2 sample weaker despite the pore compaction. In gCO_2 condition, rate of calcium carbonate formation is lower compared to $scCO_2$ that could be proved with the formation of greater amount of calcium carbonate in
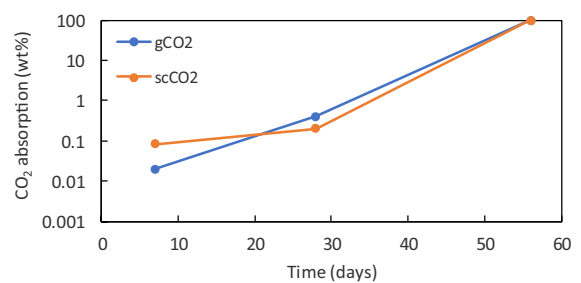
Fig. 7 CO_2 absorption rate with curing period

Geomech. Geophys. Geo-energ. Geo-resour. (2022) 8:160

Page 7 of 12   160
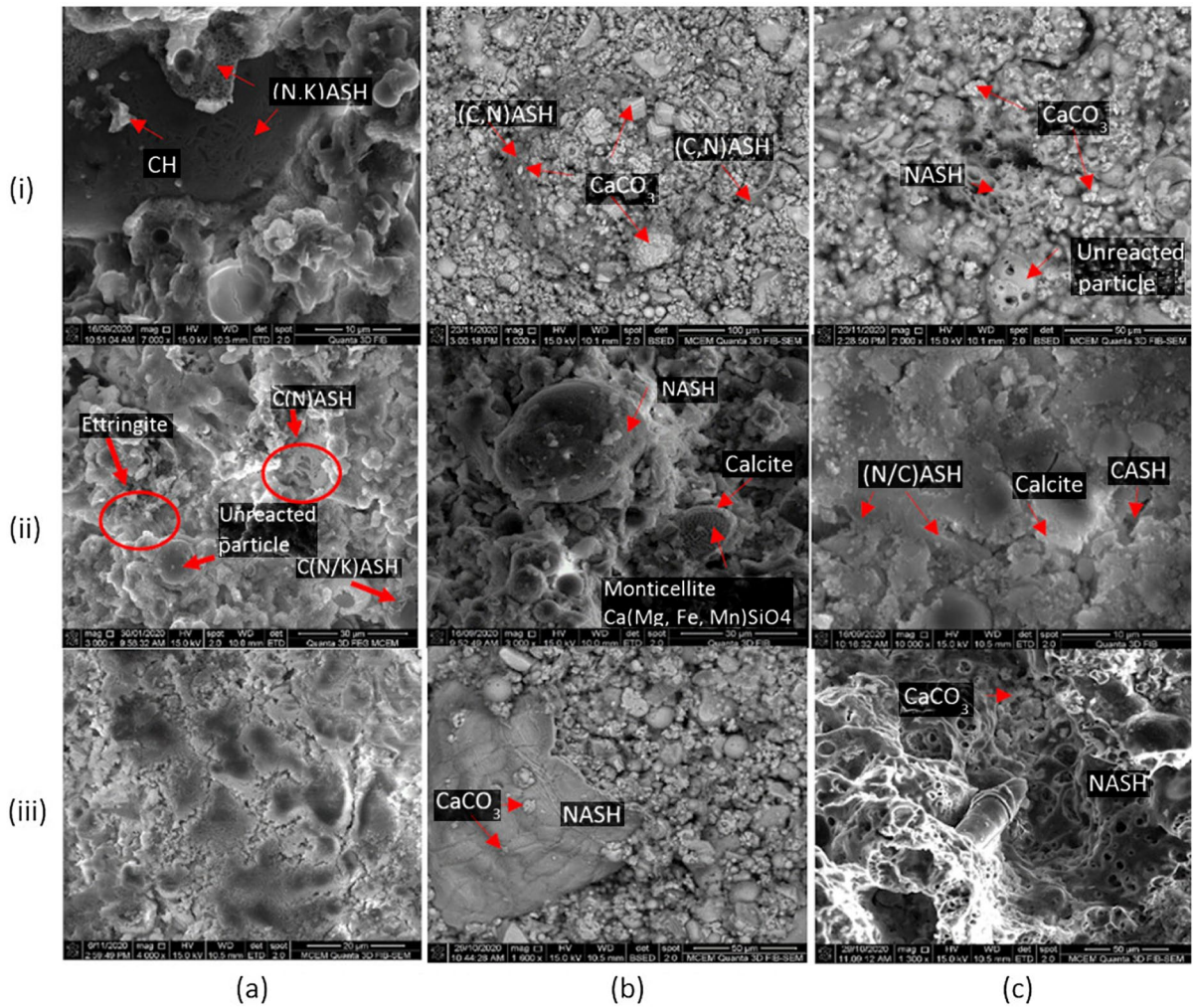
Fig. 8 SEM images of **a** control, **b** gCO$_2$-exposed, and **c** scCO$_2$-exposed samples, after (i) 7 days, (ii) 28 days, and (iii) 56 days
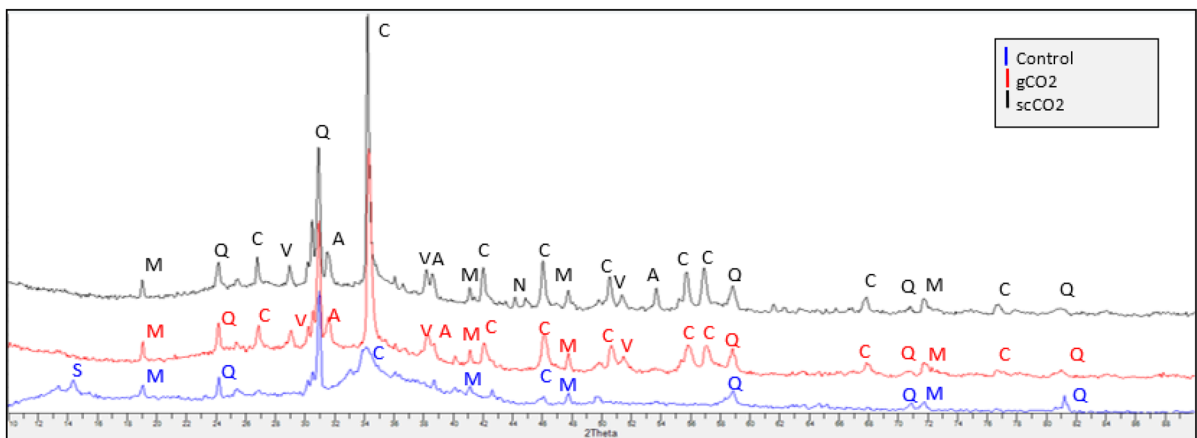
Fig. 9 XRD analysis of Composite with CO$_2$ exposure

$scCO_2$ compared to gCO_2. Generally, CO_2 initially dissolves into water, then forms carbonic acid, and reacts with cement reaction products. When CO_2 is in liquid form it is more convenient to dissolve into water and reacts with cement than gaseous CO_2. Therefore, the reaction rate in $scCO_2$ conditions is higher than gCO_2.

With $scCO_2$, vaterite, and aragonite, mineral phases are evident through X-ray Diffraction analysis in Fig. 9, but we found less vaterite in the gCO_2 condition. No aragonite was found with gCO_2, as

Mg^{2+} ions in pores were absorbed and hydrotalcite – $Mg_6Al_2CO_3(OH)_{16}\cdot4H_2O$ – was formed, which retards aragonite formation (Li et al., 2017). Vaterite and aragonite are metastable calcium carbonates, with hexagonal and orthorhombic crystal structures respectively. Formation of aragonite only occurs in $scCO_2$, because the specific samples were kept at a higher temperature (40 °C) (Maciejewski et al., 1994).

Here S = sodium calcium aluminium silicate hydrate ($Na_2O.CaO.Al_2O_3.SiO_2.H_2O$), C = calcite
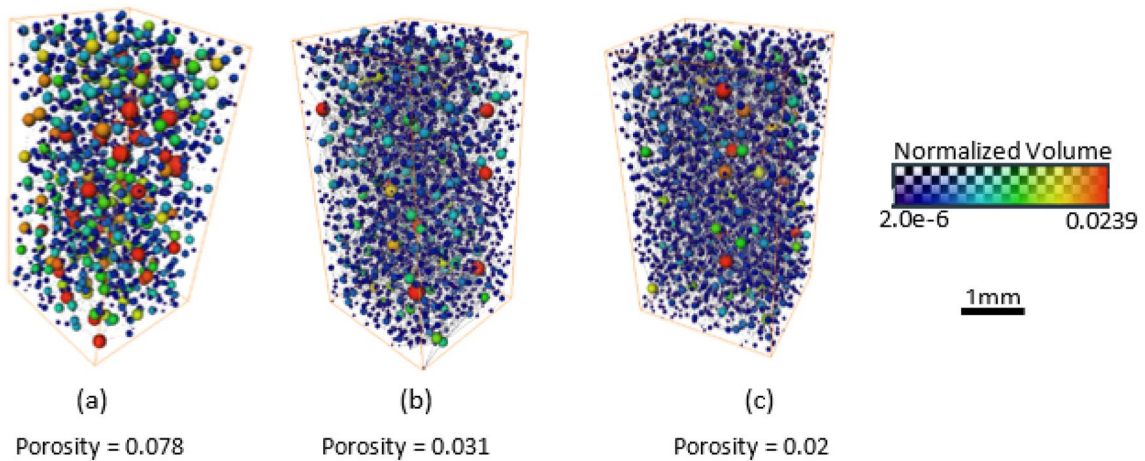
Fig. 10 Micro CT-scan images of **a** Control; **b** gCO_2; **c** $scCO_2$ samples
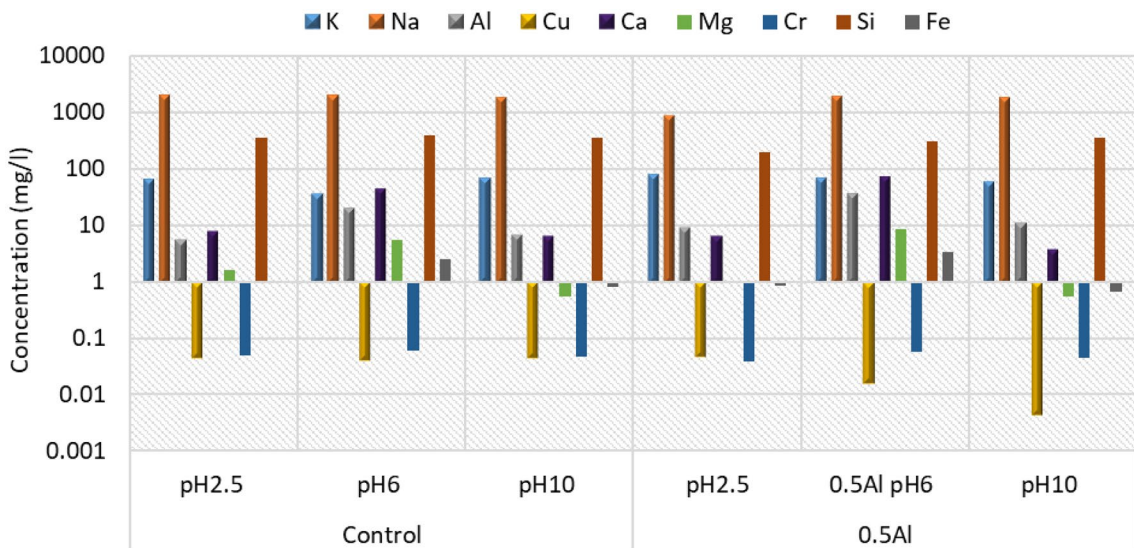
Fig. 11 Heavy-metal leaching effect with Al addition at pH 2.5, 6, and 10, after 7 days

Geomech. Geophys. Geo-energ. Geo-resour. (2022) 8:160

Page 9 of 12   **160**

($CaCO_3$), Q = quartz (SiO_2), M = mullite (Al_2O_3. SiO_2), V = vaterite ($CaCO_3$), A = aragonite ($CaCO_3$)

Eventually, both carbon-curing conditions reduced the porosity of composites by 60–74%. The volume fraction obtained from micro-CT scanning with resolution of 3.37 μm proves the effect of pore compaction with carbonation in Fig. 10, as does the SEM image (Fig. 8(c)ii).

3.4 Environmental analysis

3.4.1 Heavy metal leaching

We added nitric acid to leachates immediately after carbonation, and gas bubbles confirmed the presence of carbonates, or bicarbonate ($NaHCO_3$).

Figure 11 compares the effects of Al on heavy-metal leaching behaviour after 7 days in acidic (pH 2.5), atmospheric (pH 6), and alkali (pH 10) conditions. We found that addition of 0.5Al favours the formation of alumina gel, compacting the pores and reducing leaching of Si^{4+} by 47%, and of Na^+ by 56%.

As shown in Fig. 12, introducing CO_2 into cement significantly limits the leaching of Al^{3+}, Si^{4+}, and Na^+ into the surrounding medium. For instance, we observed significant leaching (40–67 ppm) of Al^{3+} over 7–56 days of water-curing, but almost none (<0.1 mg/l) was recorded after introducing $scCO_2$ into the medium. In $scCO_2$-saturated cement, the presence of calcite and aragonite was high compared to the water-cured composite. These carbonates act as a barrier that reduces permeability and limits leaching (Omosebi et al., 2016).

On the other hand, there was some leaching of Mg^{2+} ions in the $scCO_2$ condition during carbonation, though this condition limits leaching to relatively few ions. In the gCO_2 condition, formation of hydrotalcite limits Mg^{2+} leaching; but high crystallization of aragonite in $scCO_2$ retards the formation of hydrotalcite, so free Mg^{2+} ions in pores can leach out. However, the recorded maximum amount for Mg^{2+} ions leaching was 40% lower than the standard limit values (ARMCAPCNZ, 2000).

3.4.2 Emissions of CO_2 into the environment

We conducted comparative CO_2 emission and cost analyses for producing 1 m³ 0.5Al slurry versus 1 m³ Portland Cement slurry. We considered transportation and electricity as main factors for estimating the cost and emission for discarded Al foil. Our analysis showed that the proposed composite emits 55% less CO_2 and can be produced at 35% less cost than standard Portland cement.

As a significant side-benefit of our processing method, when we add Al foil to NaOH it produces 800 g of pure hydrogen gas for each 1 m³ of cement slurry, as shown in Eqs. 1–2. Demand for hydrogen gas, a clean and versatile fuel, has continued to rise since 1975. Annual global hydrogen production has reached around 70 million tonnes ((IEA), 2019a),
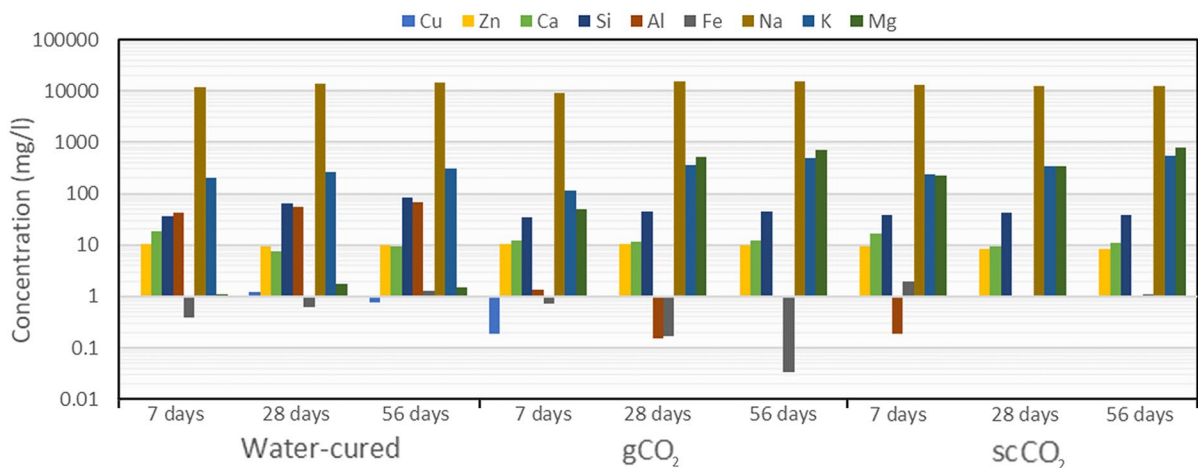
Fig. 12 Effect of carbonation on the leaching of ions, as concentration in the surrounding medium

Table 3 Comparative emission and cost analysis of 0.5Al composite and Portland Cement slurry

	Emission (kg CO_2-e/t)	Unit cost ($/t)	Mass (kg/m³)	Total emission (kg CO_2)	Total cost ($)	References
0.5Al						
FA	9	40	358	3.2	14.3	(Chen et al., 2010; Gastaldini et al. 2009)
GBFS	19	85	537	10.2	45.6	(Chen et al., 2010; Gastaldini et al. 2009)
RHA	157	225	54	8.5	12.2	(Gastaldini et al., 2009; Hu et al. 2009)
NaOH	1915	300	163	312.2	48.9	(Perez-Cortes & Escalante-Garcia, 2020; Turner & Collins, 2013)
Water	0.3	2.3	535	0.2	1.2	(Chiaia et al., 2014; TeamPoly, 2018)
Discarded Al foil	0.2	0.5	4.5	0.0009	0.0023	(EPA, 2020; Transport, 2020)
Totals:				∼334.3	∼122.2	
Portland cement						
Portland Cement	820	200	917	752	183.4	(Collins, 2010; Gastaldini et al., 2009)
Water	0.3	2.3	440	0.13	1.0	(Chiaia et al.,2014; TeamPoly, 2018)
Totals:				753.13	183.4	

but this production is only equivalent to 6% of global natural gas consumption and 2% of coal consumption, which jointly emit a yearly 830 million tonnes of CO_2. Setting yearly global cement demand at 4.1 billion tonnes ((IEA), 2020), meeting this demand by the use of our process could reduce annual emissions of CO_2 by 35 million tonnes. Producing hydrogen gas from municipal waste (Al foil) therefore appears to be a powerful adjunct in the reduction of atmospheric CO_2, as well as directly reducing landfill. Table. 3.

$$2Al + 6H_2O + 2NaOH \rightarrow 2NaAl(OH)_4 + 3H_2 \qquad (1)$$

$$2Al + 6H_2O - Al(OH)_3 + 3H_2 \qquad (2)$$
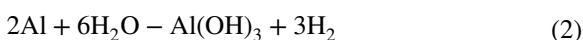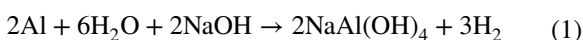
4 4. Conclusions

Through careful experimentation, we explored the development of a low-energy *greener cement* which would make best use of industrial and municipal wastes that are problematic for the recycling industry. Major benefits from this innovation are: (1) optimised reuse of waste materials; (2) reduction of CO_2 emissions from cement production; (3) absorption of atmospheric CO_2 into permanent storage in cement composite fillers; and (4) collateral production of

hydrogen gas, a promising future energy source, without the CO_2 emissions that accompany its conventional production. The product promises wide applicability in the construction industry, offering good mechanical properties and superior environmental performance compared to conventional Portland cement.

1. Major municipal waste, aluminium foil were tested in this study as substitutes for energy-consuming commercial additives, to improve the mechanical performance of cement. Though addition of 0.5% aluminium (0.5Al) limits workability, it enhances the formation of alumina gel, yields a denser composite with fewer pores, improves the compressive strength by (73-77) %, and helps to reduce leaching of Na^+ and Si^{4+}. Utilization of discarded foil minimises the greenhouse gas emitting from conventional hydrogen gas production and further, it limits the emission from the commercial additives production chain.

2. Inclusion of liquid CO_2 in water medium favours the load bearing capacity of cement by increasing the compressive strength by 10% at end of 56 days. Since, in $scCO_2$, formation of three different types of calcium carbonate; calcite, vaterite and aragonite helps to pack the pores and resists the load. However, compressive strength

Geomech. Geophys. Geo-energ. Geo-resour. (2022) 8:160

Page 11 of 12   **160**

of cement cured in gCO_2 conditions is affected due to the degradation of CSH.

3. Heavy-metal leaching from cement is a well-known environmental challenge for the industry. When our *greener cement* absorbs CO_2 (carbonation), the carbonates it forms compact the pores and reduce porosity. The supercritical CO_2- ($scCO_2$)-cured samples had significantly more calcium carbonate (calcites, aragonite), and showed less porosity than gaseous CO_2- (gCO_2)-cured samples. Due to this reduced porosity, carbonation significantly limits the movement and leaching of heavy metal ions (Al^{3+}, Si^{4+}, and Na^+). Compared to gCO_2, the $scCO_2$ condition makes a stronger barrier to limit leaching due to a higher presence of carbonates. Leaching of Mg^{2+} ions is higher with $scCO_2$; but because delayed aragonite crystallization facilitates the formation of hydrotalcite, the concentration of Mg^{2+} ions presence in leachate is 40% less than the standard limit values.

4. A 0.5Al slurry emits 55% less CO_2 than conventional Portland cement slurry, and is 35% cheaper to produce. Moreover, hydrogen (pre-eminent as a zero-carbon fuel) is released when the Al foil combines with NaOH, promising as much as 35 million tonnes net reduction in global CO_2 emissions from hydrogen fuel production alone. And finally, wide adoption of CO_2 as a cement admixture could reduce atmospheric CO_2 by 72 million tonnes annually.

References

Amato I, (2013) CONCRETE. Nature, 494.

ARMCANZ A, a. (2000) Australian and New Zealand Guidelines for Fresh and Marine Water Quality.

Aslani F, Wang L (2019) Fabrication and characterization of an engineered cementitious composite with enhanced fire resistance performance. J Clean Prod 221:202–214

Castillo H, Collado H, Droguett T, Sánchez S, Vesely M, Garrido P, Palma S (2021) Factors Affecting the Compressive Strength of Geopolymers: A Review. Minerals 11(12):1317

Chen C, Habert G, Bouzidi Y, Jullien A, Ventura A (2010) LCA allocation procedure used as an incitative method for waste recycling: An application to mineral additions in concrete. Resour Conserv Recycl 54(12):1231–1240

Cheng-Yong H, Yun-Ming L, Abdullah MMAB, Hussin K (2017) Thermal Resistance Variations of Fly Ash Geopolymers: Foaming Responses. Sci Rep 7(1):45355

Chiaia B, Fantilli AP, Guerini A, Volpatti G, Zampini D (2014) Eco-mechanical index for structural concrete. Constr Build Mater 67:386–392

Churkina G, Organschi A, Reyer CPO, Ruff A, Vinke K, Liu Z, Reck BK, Graedel TE, Schellnhuber HJ (2020) Buildings as a global carbon sink. Nature Sustainability 3(4):269–276

Collins F (2010) Inclusion of carbonation during the life cycle of built and recycled concrete: influence on their carbon footprint. The International Journal of Life Cycle Assessment 15(6):549–556

Davis SJ, Lewis NS, Shaner M, Aggarwal S, Arent D, Azevedo IL, Benson SM, Bradley T, Brouwer J, Chiang YM, Clack CTM, Cohen A, Doig S, Edmonds J, Fennell P, Field CB, Hannegan B, Hodge BM, Hoffert MI, Ingersoll E, Jaramillo P, Lackner KS, Mach KJ, Mastrandrea M, Ogden J, Peterson PF, Sanchez DL, Sperling D, Stagner J, Trancik JE, Yang CJ, Caldeira K (2018) Net-zero emissions energy systems. Science. https://doi.org/10.1126/science.aas9793

EPA (2020) Emission Factors for Greenhouse Gas Inventories.

Fawer M, Concannon M, Rieber W (1999) Life cycle inventories for the production of sodium silicates. Inter J Life Cycle Assessment 4(4):207

Gastaldini ALG, Isaia GC, Hoppe TF, Missau F, Saciloto AP (2009) Influence of the use of rice husk ash on the electrical resistivity of concrete: A technical and economic feasibility study. Constr Build Mater 23(11):3411–3419

Habert G, Miller SA, John VM, Provis JL, Favier A, Horvath A, Scrivener KL (2020) Environmental impacts and decarbonization strategies in the cement and concrete industries. Nature Reviews Earth & Environment 1(11):559–573

160 Page 12 of 12

Geomech. Geophys. Geo-energ. Geo-resour. (2022) 8:160

Hu M, Zhu X, Long F (2009) Alkali-activated fly ash-based geopolymers with zeolite or bentonite as additives. Cement Concr Compos 31(10):762–768

(IEA) I. E. A., (2018) Cement technology roadmap plots path to cutting CO2 emissions 24% by 2050.

(IEA) I. E. A., (2019a) The Future of HydrogenIEA, P.

(IEA) I. E. A., (2019b) Global Status Report for Buildings and Construction 2019b.Paris.

(IEA) I. E. A., (2020) CementIEA, P.

Inc Si, (2017) Specification of Aluminium Foil.

Khalifeh M, Saasen A, Vralstad T, Hodne H (2014) Potential utilization of class C fly ash-based geopolymer in oil well cementing operations. Cement Concr Compos 53:10–17

Kim TY, Hwang K-Y, Hwang I (2016) Strength Development and Carbonation Characteristics of Slag Cement/Class C Fly Ash blended CO 2 Injection Well Sealant. Journal of Soil and Groundwater Environment 21(2):29–37

Latawiec R, Woyciechowski P, Kowalski K (2018) Sustainable Concrete Performance–CO2-Emission. Environments 5(2):27. https://doi.org/10.3390/environments5020027

Li N, Farzadnia N, Shi C (2017) Microstructural changes in alkali-activated slag mortars induced by accelerated carbonation. Cem Concr Res 100:214–226

Maciejewski M, Oswald HR, Reller A (1994) Thermal transformations of vaterite and calcite. Thermochim Acta 234:315–328

Mi T, Li Y, Liu W, Li W, Long W, Dong Z, Gong Q, Xing F, Wang Y, (2021) Quantitative evaluation of cement paste carbonation using Raman spectroscopy. npj Materials Degradation, 5(1), 35.

Mohajerani A, Suter D, Jeffrey-Bailey T, Song T, Arulrajah A, Horpibulsuk S, Law D (2019) Recycling waste materials in geopolymer concrete. Clean Technol Environmental Policy 21(3):493–515. https://doi.org/10.1007/s10098-018-01660-2

Mohammed AS (2018) Vipulanandan model for the rheological properties with ultimate shear stress of oil well cement modified with nanoclay. Egypt J Pet 27(3):335–347

Omosebi O, Maheshwari H, Ahmed R, Shah S, Osisanya S, Hassani S, DeBruijn G, Cornell W, Simon D (2016) Degradation of well cement in HPHT acidic environment: Effects of CO2 concentration and pressure. Cement Concr Compos 74:54–70

Osman A (2017) (2017) Breakthrough' sees waste aluminium foil used to produce biofuel. Belfast Telegraph 26:2017

Patel M, Bastioli C, Marini L, Würdinger E, (2005) Life-cycle Assessment of Bio-based Polymers and Natural Fiber Composites, Biopolymers Online.

Perez-Cortes P, Escalante-Garcia JI (2020) Alkali activated metakaolin with high limestone contents – Statistical modeling of strength and environmental and cost analyses. Cement Concr Compos 106:103450

Richard A. Clarke RNS, Ladd GJ, Joan LB, Frances C, Daniel CE, Bruce S, Johan P, Richard PW, Rob G, Kurt F, Johan S, (1994) The Challenge of Going Green, Sustainability1994.

Şahmaran M, Özbay E, Yücel HE, Lachemi M, Li VC (2011) Effect of fly ash and PVA Fiber on microstructural damage and residual properties of engineered cementitious composites exposed to high temperatures. J Mater Civ Eng 23(12):1735–1745

Scrivener KL, Capmas A (1998) 13 - Calcium Aluminate Cements. In: Hewlett PC (ed) Lea's Chemistry of Cement and Concrete, 4th edn. Butterworth-Heinemann, Oxford, pp 713–782

Sun X, Wu Q, Zhang J, Qing Y, Wu Y, Lee S (2017) Rheology, curing temperature and mechanical performance of oil well cement: Combined effect of cellulose nanofibers and graphene nano-platelets. Mater Des 114:92–101

TeamPoly (2018) Water Prices in Australia, 2018. Available online: [Accessed.

Transport DO, (2020) Owner- Drivers (Contracts and Disputes) ACT 2007.

Turner LK, Collins FG (2013) Carbon dioxide equivalent (CO2-e) emissions: A comparison between geopolymer and OPC cement concrete. Constr Build Mater 43:125–130

Venkatanarayanan HK, Rangaraju PR (2015) Effect of grinding of low-carbon rice husk ash on the microstructure and performance properties of blended cement concrete. Cement Concr Compos 55:348–363

Wan H, Liqun Yuan Yu, Zhang, (2020) Insight Into the Leaching of Sodium Alumino-Silicate Hydrate (N-A-S-H) Gel: A Molecular Dynamics Study. Frontiers in Mater. https://doi.org/10.3389/fmats.2020.00056